Dynamic finite-element simulations reveal early origin of complex human birth pattern

Pierre Fremondiere (pierrefremondiere@yahoo.fr)
Aix Marseille University, CNRS/EFS, UMR 7268, and School of Midwifery, Faculty of Medical and Paramedical Sciences https://orcid.org/0000-0003-2800-4217

Lionel Thollon
Aix Marseille University, UMR-T24, Marseille, France.

François Marchal
Aix Marseille University, CNRS, EFS, ADES, Marseille, France.

Cinzia Fornai
University of Zurich https://orcid.org/0000-0002-0911-0164

Nicole Webb
Senckenberg Research Institute and Natural History Museum Frankfurt, Senckenberganlage 25, 60325 Frankfurt am Main, Germany.

Martin Haeusler
University of Zürich https://orcid.org/0000-0002-9100-4183

Article

Keywords: human birth pattern, finite-element birth simulations, australopithecines

Posted Date: August 16th, 2021

DOI: https://doi.org/10.21203/rs.3.rs-609827/v1

Version of Record: A version of this preprint was published at Communications Biology on April 19th, 2022. See the published version at https://doi.org/10.1038/s42003-022-03321-z.

Dynamic finite-element simulations reveal early origin of complex human birth pattern

Authors: Pierre Frémondière[1,2]*, Lionel Thollon[3], François Marchal[2], Cinzia Fornai[4,5], Nicole M. Webb[4,6], Martin Haeusler[4]*

Affiliations:

[1]Aix Marseille University, CNRS, EFS, ADES, Marseille, France.

[2]Aix Marseille University, School of Midwifery, Faculty of Medical and Paramedical Sciences, Marseille, France.

[3]Aix Marseille University, UMR-T24, Marseille, France.

[4]Institute of Evolutionary Medicine, University of Zuerich, Winterthurerstrasse 190, 8057 Zürich, Switzerland.

[5]Department of Evolutionary Anthropology, University of Vienna, Althanstrasse 14, 1090 Wien, Austria.

[6]Senckenberg Research Institute and Natural History Museum Frankfurt, Senckenberganlage 25, 60325 Frankfurt am Main, Germany.

*Correspondence to: pierre.fremondiere@univ-amu.fr; martin.haeusler@iem.uzh.ch

Abstract (147 of 150 words)

Human infants are born neurologically immature, but whether this originates from conflicting selection pressures between bipedal locomotion and encephalization as suggested by the obstetrical dilemma remains controversial. Australopithecines are ideal for investigating this

trade-off as they have a bipedally adapted pelvis, yet relatively small brains. Our finite-element birth simulations based on different pelvic reconstructions and a range of fetal head sizes indicate that australopithecines already possessed a human-like rotational birth pattern. Since only newborn head sizes smaller than those predicted for non-human primates leave adequate space for soft tissue between the bony pelvis and fetal skull, our data imply that australopithecines had secondarily altricial newborns and likely evolved cooperative breeding to care for their helpless infants. These prerequisites for advanced cognitive development therefore seem to have been corollary to skeletal adaptations to bipedal locomotion that preceded the appearance of the genus *Homo* and the increase in encephalization.

Introduction

While passing through the tight, convoluted birth canal the human fetus follows a curved trajectory formed by the lumbar and sacral curves of the mother's vertebral column, and typically needs to flex and rotate its head at various stages[1]. This process can be hazardous for both the fetus and the mother and thus commonly requires the assistance of birth attendants, which contrasts to the generally faster and uncomplicated delivery of most other mammals[2,3]. As an adaptation, human neonates are born physically and neurologically more immature with smaller brains relative to those of adults compared to non-human primates. This condition is known as secondary altriciality as it is convergent in some aspects to altriciality, the ancestral life history trait of mammals which is retained, e.g., in carnivores and many rodents[4]. However, in contrast to these species, human gestation length is not truncated and newborns are basically precocial as in all primates[5,6]. The emergence of this human-like birth pattern has been attributed to opposing selection pressures related to encephalization and the changes facilitating biomechanical efficiency during bipedal

locomotion, which has dramatically reshaped the pelvis over the course of hominin evolution[7].

This alleged trade-off, known as the obstetrical dilemma, is notoriously difficult to test and has recently been challenged on multiple fronts[8-12]. Here, we employ an evolutionary approach focusing on australopithecines, the earliest known hominins with well-preserved pelvic remains to explore the origins of the complex birth psttern characteristic of modern humans. While retaining relatively small brain sizes[13], australopithecines already demonstrate a shortened distance between the sacroiliac and hip joints similar to modern humans which reduced torque during upright bipedalism but ultimately constrained the size of the birth canal. Analyses using australopithecines therefore permit differentiation between obstetrical adaptations explicitly relating to bipedal locomotion from those related to our large brain size.

Previous attempts to reconstruct the evolution of human birth yielded conflicting results because of different estimates for fetal head size and different reconstructions of pelvic canal shape[14-20] while the soft tissue within the birth canal was rarely taken into account[16]. Most studies either used skull dimensions of a newborn chimpanzee[14,15,18] (although australopithecines had with 420–459 cm^3 a slightly larger mean adult brain volume than the 369 cm^3 of chimpanzees[21]; Table S1), or estimates based on adult brain size[16,20]. Non-human primates, including great apes, have a neonatal brain size that is on average 43% of adult brain size, while this ratio is only 28% in modern humans[22]. It is controversial whether this different neonatal-to-adult brain size proportion can simply be explained by allometry[23], or whether humans have a relatively smaller newborn brain size due to secondary altriciality[22]. Using the scaling relationship of neonatal-to-adult brain size based on 27 primate species[22], mean neonatal brain mass for *Australopithecus afarensis, A. africanus* and *A. sediba* is estimated to a range of 166–184 g (Extended Data Table 1). In contrast,

using the ratio typical of modern humans, a mean neonatal brain size of between 111 g and 121 g is predicted for *Australopithecus*. On the other hand, a regression equation based on seven catarrhine primates including humans[23] predicts neonatal brain sizes that are slightly smaller than those predicted from the general primate formula.

For this study, we scaled a fetal head model to three different neonatal brain sizes: 180 g, corresponding to a submaximal brain size using a general primate neonatal-to-adult brain size ratio; 110 g, which is close to the minimum predicted brain size using a modern human ratio; and an intermediate value of 145 g (Fig. 1). To account for the complex shape of the pelvis, the dynamic nature of childbirth, and the unique reaction forces resulting from fetopelvic contact, we performed a dynamic 3D finite-element simulation of the birth process in australopithecines (Fig. 2), considering all published pelvic reconstructions. We also simulated sacro-iliac joint laxity, which typically occurs in all primates including humans[24]. The resulting cephalopelvic gap between the bony pelvic canal and the fetal skull was then compared to values for fetopelvic soft-tissue thickness derived from human intrapartum MRI scans and sonographic measurements (see Methods). The suitability of the bony pelvic shape for predicting fetal head rotation was assessed with a birth simulation based on a modern human pelvis.

Results and discussion

Our bony finite element simulations showed a similar outcome for all published australopithecine pelvic reconstructions, suggesting that overall pelvic shape was of minor importance compared to the actual dimensions of the birth canal relative to fetal head size. In fact, all three known female australopithecine pelves are of small body size and have a comparably large birth canal cross-sectional area, including A.L. 288-1 (*Australopithecus*

afarensis, dated to 3.18 Ma), Sts 14 (*A. africanus*, 2.6-2.1 Ma), and MH2 (*A. sediba,* 1.98 Ma) (Fig. 3, Table 1).

All simulations using a 180 g fetal brain size resulted in a dystocic birth. The descent stopped at either the inlet or midplane even when the biparietal diameter of the fetal skull was slightly smaller than the anteroposterior diameter of the pelvis due to the eccentric alignment of the fetal head with the heart-shaped pelvic canal (Fig. 4, Extended Data Fig. 1-8). A mid-arrest was observed in our bony birth simulation of the two mother-infant dyads of Sts 14 with a 180 g brain size (Table 1, Extended Data Fig. 1). All other australopithecine pelves allowed the passage of a 145 g fetal brain size except for Lovejoy's[25] reconstruction of A.L. 288-1, which possessed the smallest anteroposterior diameter. The pelvic constriction was slightly relieved after scaling the model to the dimensions published by Tague & Lovejoy[14] (see Methods). All simulations with a 110 g fetal head size resulted in an eutocic birth.

Our in silico simulations confirmed previous studies[14,20] that were based on chimpanzee-sized fetal skulls (corresponding to a ca. 155 g = 162 cm^3 brain size) by finding no direct bony obstruction in A.L. 288-1 (*A. afarensis*) or MH2 (*A. sediba*). However, we observed a minimum gap of only 0.7–4.1 mm between the external bony surface of a 155 g fetal head and the maternal pelvic inlet of these reconstructions. With the 145 g fetal head that we used in our FEA simulations, this cephalopelvic gap increased to 0.9–4.5 mm in A.L. 288-1, to 5.9–6.2 mm in Sts 14, and to 3.2–5.1 mm in MH2, while with a 110 g fetal head, the gap became 3.9–7.5 mm in A.L. 288-1, 7.6–8.6 mm in Sts 14, and 8.0 mm in MH2 (Table 1). This contrasts to the average thickness of about 10.6 mm (associated with the need for a Caesarean section) to 12.6 mm to which the soft tissue of the birth canal is compressed during vaginal delivery in modern humans[26] (see Methods). Consistent with this, we observed a fetopelvic soft tissue thickness in the midsagittal plane of 11.3 mm in our birth simulation of an average modern human female pelvis paired with an average sized fetal

skull (Extended Data Fig. 9). Adjusting for the smaller body size of australopithecines, this suggests a minimum fetopelvic soft tissue thickness of about 7.0–10.6 mm in these early hominins. Using the lower end of the predicted range of minimum fetopelvic soft tissue thickness (which is based on values observed with Caesarean sections in modern humans) in combination with the size and shape of the birth canal, this implies that *Australopithecus* had an average neonatal brain size closer to 110 g than to 145 g.

In humans, the fetal head often undergoes significant deformation caused by cranial moulding during birth. This typically leads to a reduction of the vertical diameter and a concomitant elongation of the occipitofrontal diameter, while biparietal breadth remains nearly unaffected[27,28]. Conversely, substantial moulding has not been reported for non-human primates, which is likely due to the more advanced closure of the fontanels and cranial sutures at birth[24,29]. In addition, high-resolution CT scans of the Taung skull provide no evidence of delayed fusion of cranial sutures in australopithecines[30]. In our simulations with a dystocic outcome, the greatest compressive stresses were observed laterally at the parietal bones of the australopithecine fetal skulls. This is, however, a dimension that is barely affected by moulding since substantial deformation of fetal head breadth is not possible in primates due to the rigidity of the basicranium. Thus, even if fetal head moulding would have already been present in *Australopithecus*, the passage of a fetus with an average brain size of 145 g or larger would have been difficult, if not impossible.

In smaller quadrupedal primates with relatively large fetal heads compared to the maternal pelvic dimensions such as *Papio* and *Saimiri* (and other small mammals), the symphysis can open to increase pelvic inlet area up to 30% and 100%, respectively[24]. In contrast, ligamentous laxity at the symphysis seems to be negligible in great apes and humans given that the two hipbones often fuse in chimpanzees at the symphysis in both sexes[31,32] whilst in humans the symphysis widens on average by only 3 mm towards the end of

pregnancy, rendering the inlet as a virtually undeformable bony ring[24,33]. This rigidity seems to be related to the greater body size and bipedal locomotion of great apes and modern humans, respectively, which increases shearing stress at the pubic symphysis. Furthermore, MRI studies have demonstrated that the utilization of non-supine birth positions such as kneeling-squatting reduces, rather than increases, the diameters of the pelvic inlet[34,35]. In clinical practice, this makes the inlet particularly prone to arrest of labour due to fetopelvic incongruence despite sufficient uterine contractions. Without assistance, this would provoke obstetric disorders ranging from urogenital fistulas to uterine rupture[1]. On the other hand, and in contrast to the inlet, both anteroposterior and transverse diameters of the pelvic midplane and outlet can be significantly increased thanks to sacro-iliac joint mobility, particularly in non-supine birth positions[1,34,35]. Birth might therefore still be possible—albeit difficult—in the event of a mid-arrest, as we observed it in one birth simulation in Sts 14 (Table 1).

All bony finite element simulations with an eutocic outcome showed a rotation of the fetal head during the descent if they started from a left occiput anterior (LOA) head position at the pelvic inlet, which is typical for modern humans. The only exception was the dyad of a 110 g fetal head size and the reconstruction of A.L. 288-1 by Brassey et al.[17]. In that particular dyad, the fetal skull did not get into contact with the pelvis due to the relatively straight pelvic canal, and rotation was consequently not induced. The majority of our australopithecine reconstructions showed a transverse fetal head orientation at the pelvic outlet (Table 1). However, this appears to be an artefact of the absence of soft tissue in these models. In fact, also a bony birth simulation for a modern human female with average pelvic and fetal head dimensions showed an anomalous 45° rotation of the fetal head into a transverse orientation at the pelvic outlet. Such transverse positions are unusual in primates and more generally in mammals. They are not only associated with shoulder dystocia in modern humans, but given the sagittal orientation of the muscle fibres of the pelvic floor, this

position is also linked to birth difficulties, particularly excessive stretching of the perineum and severe perineal tears[1,18,24]. Our results therefore suggest that the exact amount of fetal head rotations in the lower sections of the birth canal cannot reliably be simulated based on bony morphology alone. Another factor is the nearly circular cross-section of the flexed (but also of the fully extended) fetal head, so that the exact shape of the skull is of minor importance. The choice to utilize a fetal head model based on a newborn modern human or a chimpanzee is therefore irrelevant in such simulations (Extended Data Fig. 10), and FEA models that incorporate the maternal pelvic floor musculature and the infant's shoulders, along with forces simulating uterine contractions, would be required to accurately predict the fetal head orientation at the pelvic outlet. These findings challenge the outcome of previous studies suggesting a transverse position of the fetal head at the pelvic outlet in *Australopithecus*[14,20].

Our results imply that *Australopithecus* already evolved neonatal-to-adult brain size proportions similar to those of modern humans, whereas it seems unlikely that these early hominins could have delivered newborns with relative brain sizes characteristic of great apes. Australopithecines therefore seem to have resembled humans in being secondarily altricial to diminish the risk of cephalopelvic constraints. Independent support for neurologically immature newborns in australopithecines compared to those of non-human primates comes from the almost human-like, slow brain growth pattern reported for the 2.4-year-old DIK 1/1 (*A. afarensis*) child[21]. This protracted brain growth has originally been interpreted within the framework of the metabolic hypothesis of human altriciality[21]. According to this so-called Energetics of Gestation and Growth (EGG) hypothesis, the relatively small brain size at birth in humans is the result of a limitation of the energy the mother can invest in fetal growth during pregnancy[12] since the brain is the energetically most expensive tissue of the body[36]. However, because brain size in australopithecines was only marginally larger relative to body

mass than that inferred for our common ancestor with chimpanzees[13], it is difficult to imagine that metabolic reasons alone would have prevented these early hominins form giving birth to infants with brain sizes of 166–184 g as predicted from newborn-to-adult brain size proportions of a general primate model. Our findings therefore support the original obstetrical dilemma hypothesis[7] that secondary altriciality in hominins is related to the increased cephalopelvic constraints associated with the anteroposterior shortening of the birth canal as an adaptation to bipedalism, although some combination of these two hypotheses might also be conceivable[6].

Whereas the birth trajectory of chimpanzees is nearly straight, a recent study revealed a similarly tight cephalopelvic fit with a gap between the bony pelvis and the fetal skull that is only 1–2 mm wider than on average in modern humans[37]. Consequently, already a slightly reduced anteroposterior pelvic diameter and an increased curvature of the birth trajectory would have substantially intensified the obstetric selection pressures in early hominins. Evidence for this is also provided by the presumed male australopithecine pelvic remains discovered in the last decades such as KSD-VP 1/1, StW 431, Sts 65, and MH1 that all possess a narrower greater sciatic notch compared to A.L. 288-1, Sts 14 and MH2[19,38,39]. This higher degree of sexual dimorphism in pelvic shape compared to great apes has been argued to be an adaptation to mitigate the obstetric consequences of a convoluted, tight birth canal[2,6,40].

Neurologically immature australopithecine infants required more assistance, including the need to be actively carried for a prolonged period after birth, suggesting that behaviours like provisioning and cooperative care may already have been initiated at this early stage of human evolution before the appearance of the genus *Homo* (Fig. 5). Cooperative breeding has been argued to represent the most plausible exaptation for brain size increase in hominins[41,42]. Such elaborate social behaviours likely established a trend towards prolonged cognitive

development that was crucial for the eventual acquisition of human-like intellectual capabilities[43,44], and it provided an apt environment for the manufacturing of the earliest documented stone tools 3.3 Ma ago[45]. Consequently, our results suggest that the restructuring of the pelvis due to bipedalism created the selection pressure leading to an initial step towards a human-like life history pattern. As such, both secondary altriciality and rotational birth seem to have ensued from bipedalism rather than from encephalization itself. Hence, it was bipedalism that prepared the adaptive milieu for the drastic encephalization occurring later during the evolution of the genus *Homo*.

Materials and Methods

Finite-element analysis. The birth simulations were performed with finite-element analyses (FEA) using Radioss 11.0 (www.altair.com). Typical of modelling, this approach required simplification in order to understand the effects of various parameters while still capturing the intended phenomenon accurately. Specifically, the complexity of the dynamic birth process was reduced to a set of finite elements with solvable differential equations that can be applied to complex biological forms. Resultant forces were modelled based on the deformation of the fetal skull. This deformation is related to the different material properties and the force of descent applied to the fetal head. A free time step, i.e., an incremental time between two cycles, of 0.001 ms was considered for each calculation. The time step was decreased up to 1×10^{-6} ms when two surfaces were approaching each other. The decreasing time step permitted the management of the numerical relationship between the pelvis and the fetal head. The resulting animation was recorded at each millisecond. The total computation

time of a simulation was between 2 and 4 hours depending on the number of processors used (six to 12).

Pelvic meshes. A 3D surface scanner-generated model of Lovejoy's[25] reconstruction of A.L. 288-1 was obtained from the author. This reconstruction was said to be the same as that used by Tague & Lovejoy[14]. However, the diameters of the pelvic canal were slightly smaller than the dimensions published by Tague & Lovejoy[14] (inlet AP 73 vs. 76 mm, ML 128 vs. 132 mm, midplane AP 70 vs. 72 mm, ML 106 vs. 101 mm). We therefore scaled the 3D model of Lovejoy's[25] reconstruction by a factor of 1.046 sagittally and 1.033 mediolaterally as well as superoinferiorly to obtain the dimensions of the Tague & Lovejoy[14] reconstruction. Because there was no explanation for the discrepancy between the two, except for possible anisotropic shrinkage of the casts, both variants were used in our simulations. The manual reconstruction of A.L. 288-1 and Sts 14 by Häusler & Schmid[16] and the reconstruction of MH2 by Kibii et al.[19] (provided by P. Schmid) were scanned with a high-resolution surface scanner (PT-M4c, Polymetric GmbH, Darmstadt, Germany). Since these models also showed slight discrepancies of the birth canal dimensions to the published diameters, we also scaled them accordingly. All other pelves represent virtual reconstructions and were provided by the corresponding authors as digital models. The MH2 reconstructions by Laudicina et al.[20] and the scaled version of Kibii et al.[19] showed nearly identical dimensions of the pelvic canal. However, because the sacrum promontorium was not reconstructed by Laudicina et al.[20], only the version of Kibii et al.[19] was used in the simulations. The sacrum was then isolated from the hipbones via segmentation conducted in Geomagic (www.3dsystems.com) to enable a mobile sacro-iliac joint. All 3D models were re-meshed in Hypermesh 12.0 (www.altair.com) to generate shell elements of an average size of 1 mm and to eliminate mesh inconsistencies, duplicated faces and other artefacts.

Fetal skull meshes. Our fetal skull model used for the bony finite element simulations was based on a CT scan of a human fetus at 35 weeks of gestation (local ethics committee number: 1d-RCB 2011-A00072-39). The CT scan was performed with a 16 slice Siemens SOMATOM Definition Flash strip scanner with 0.6 mm slice thickness. The CT images were segmented in Mimics 12.3 (www.materialise.com). The generated polygonal mesh of the fetal head was re-meshed in Hypermesh 12.0 (www.altair.com) to produce 18,000 shell elements with an average size of 1 mm (Fig. 3). The fetal head model was then scaled to conform to the brain masses of 180 g, 145 g, and 110 g using the neurocranial dimensions of a chimpanzee neonate[46] (in fact, fetal neurocranial proportions of chimpanzees, humans and those predicted for Taung are almost identical)[47]. This yielded fetal heads with biparietal diameters of 75 mm, 70 mm, and 64 mm, respectively, and occipito-frontal diameters of 87 mm, 81 mm, and 75 mm, respectively.

Models and data setting. Material properties were assigned according to the fetal head model of Lapeer and Prager[48], with a Young's modulus for the stiffness of the skull bones of E = 3,800 MPa and E=200 MPa for the fontanels, which corresponds to material properties close to that of cartilage[49,50]. The power of descent of the fetal body was modelled by applying the force of gravity to the centre of the fetal head[51]. This relatively weak expulsion force was chosen to minimize deformation of the fetal skull. This model therefore closely reflects the mechanical behaviour that can be presumed for the fetal head of the common ancestor of chimpanzees and humans as well as *Australopithecus*.

Material properties of cortical bone equal to E=18,000 MPa were assigned to the hipbones and to the sacrum[52]. The Poisson's ratio ν was 0.3 for all parts and the density 2.1 g/cm^3. The hipbones and the sacrum were considered as elasto-plastic materials according to a Johnson-Cook model, while the skull and the fontanels were considered as linear elastic materials. The modulus of rigidity G was determined according to Hooke's law as G = E/2(1

+ ν). The hipbones were considered as rigid bodies fixed in all 6 degrees of freedom. The contact boundary was set to 1 mm.

During delivery, the modern human sacrum can nutate (i.e., rotate) thanks to the hormonally mediated laxity of the ligaments of the sacro-iliac joint causing a posterior displacement of its apex by up to 2 cm[53,54] (Extended Data Fig. 11). We therefore modelled the sacro-iliac junction by a spring located in the centre of the sacro-iliac joint (Fig. 3) and allowed movements only around the transverse axis with 1 degree of freedom[55]. The nutation of the sacrum was associated with an increasing resistance up to a maximum mobility of 2 cm. Thus, until 10° of rotation, the movement was free, while between 10° and 13.5° the stiffness of the rotation increased from 0.1 Nm^{-1} to 1000 Nm^{-1}, corresponding to a complete limitation of the mobility of the sacrum. We started our simulations with the fetal head in a left occiput anterior (LOA) orientation, in which the fetal head is flexed and the occiput points to the left pubis of the maternal pelvis[1].

To test our approach, we used a birth simulation for an average modern human female pelvis and a standard neonate skull. To avoid effects of relaxed selection due to the introduction of Caesarean sections[56], age-related changes in pelvic dimensions[57] and macrosomic offspring due to secular trends in obesity[58] we used fetopelvic dimensions typical for the 19th century of Central Europe. The mean pelvic inlet of 15 reproductive-aged females of the Weisbach collection (Natural History Museum Vienna) had a sagittal diameter of 116.1 mm and a transverse diameter of 136.1 mm. This collection was assembled by Augustin Weisbach (1837-1914) in the late 19th century from military personnel of the Austro-Hungarian army and thus consists of individuals of known age and sex that were fit to serve and had no pathologies affecting skeletal growth and development[59]. The model for the neonate skull (biparietal breadth 89.8 mm, occipitofrontal length 110.7 mm) was then scaled

to the dimensions of a 2-day-old CT-scanned neonate[60] matching the mean neonatal brain mass of 368 g (389 cm^3; N=79)[61,62].

Estimation of soft tissue contribution to cephalopelvic fit. During labour, soft tissue in the birth canal can be compressed by the fetal head only to a certain degree. Using intrapartum transperineal ultrasound, retropubic tissue thickness in humans during vaginal delivery (measured as the shortest distance between the outer capsule of the pubic symphysis and the outer surface of the skin of the fetal head) has been determined as 11.6±3.2 mm (N = 59), while Caesarean section was associated with a retropubic tissue thickness of 9.4±2.4 mm (N=23) [26]. To this we added the thickness of the skin of the fetal head as 1.8 mm, measured on intrapartum MRI scans[27,63,64]. Maternal soft tissue thickness in front of the sacrum is slightly thinner with 6.0 to 10 mm measured on sagittal plane intrapartum MRI scans[27,63-65], which is supported by intrapartum X-rays[28,66]. If the fetal head is centred within the birth canal, this implies a mean fetopelvic soft tissue thickness of about 10.6–12.6 mm for vaginal delivery and a lower limit of 9.5 mm (associated with Caesarean section). Given that the body mass of female australopithecines is about 40–60% of modern human females and that linear dimensions scale to the cube root of body volume and thus body mass, the average fetopelvic tissue thickness of australopithecines can be approximated to between $\sqrt[3]{0.4} \times 9.5$ mm and $\sqrt[3]{0.6} \times 12.6$ mm = 7.0 mm to 10.6 mm. The analyses of the cephalopelvic fit and fetopelvic tissue thickness was then performed in Rhinoceros 7.0 (www.rhino3d.com) based on 3D surface scans of a modern human and a chimpanzee neonate (A.H. Schultz collection, Anthropological Institute, University of Zürich) scaled to the diameters corresponding to brain masses of 180 g, 145 g, and 110 g.

Acknowledgments

We thank K. Isler and R.D. Martin for discussion. O. Lovejoy, D. Goularas P. Schmid and N. Laudicina provided their reconstructions of A.L. 288-1, Sts 14, and MH2, respectively. Access to the fossils was granted by the Ethiopian Authority for Research and Conservation of Cultural Heritage (ARCCH) and M. Endalamaw (National Museum of Ethiopia), F. Thackeray and S. Potze (Ditsong National Museum of Natural History), and B. Zipfel (Evolutionary Studies Institute, University of the Witwatersrand). For access to the modern human material we thank M. Ponce de León (Anthropological Institute, University of Zürich) and K. Wiltschke-Schrotta and S. Eggers (Natural History Museum Vienna).

Funding: This research was funded by the CNRS grants GDR 3592 and IRN Bipedal Equilibrium (P.F., L.T. and F.M.), and the Swiss National Science Foundation, grant No. 31003A-156299/1 (M.H., C.F., and N.M.W.).

Author contributions: P. F., L.T., F.M and M.H. conceived the study. P.F., M.H., F.M. and L.T. developed the method. L.T. and P.F. performed the simulations. M.H., P.F., F.M. and N.M.W. wrote the manuscript with contribution from all co-authors. **Competing interests**: Authors declare no competing interests. **Data and materials availability**: All data are available in the main text or the supplementary materials

References

1 Dudenhausen, J. W., Obladen, M. & Pschyrembel, W. *Practical Obstetrics*. (De Gruyter, 2014).

2 Rosenberg, K. & Trevathan, W. Birth, obstetrics and human evolution. *Br. J. Obstet. Gynaecol.* **109**, 1199–1206, doi:10.1016/S1470-0328(02)00410-X (2002).

3 Trevathan, W. Primate pelvic anatomy and implications for birth. *Phil. Trans. R. Soc. B* **370**, 20140065, doi:10.1098/rstb.2014.0065 (2015).

4 Martin, R. D. The evolution of human reproduction: a primatological perspective. *Am. J. Phys. Anthropol.* **Suppl 45**, 59–84 (2007).

5 Portmann, A. Die Tragzeiten der Primaten und die Dauer der Schwangerschaft beim Menschen: ein Problem der vergleichenden Biologie. *Rev. Suisse Zool.* **48**, 511–518 (1941).

6 Haeusler, M. *et al.* The obstetrical dilemma: There's life in the old dog yet. *Biological Reviews*, DOI: 10.1111/brv.12744 (2021).

7 Washburn, S. L. Tools and human evolution. *Sci. Am.* **203**, 63–75, doi:10.1038/scientificamerican0960-62schul (1960).

8 Pavličev, M., Romero, R. & Mitteroecker, P. Evolution of the human pelvis and obstructed labor: new explanations of an old obstetrical dilemma. *Am. J. Obstet. Gynecol.* **22**, 3–16, doi:10.1016/j.ajog.2019.06.043 (2019).

9 Wells, J. C. K. Between Scylla and Charybdis: renegotiating resolution of the 'obstetric dilemma' in response to ecological change. *Phil. Trans. R. Soc. B* **370**, 20140067, doi:10.1098/rstb.2014.0067 (2015).

10 Warrener, A. G., Lewton, K. L., Pontzer, H. & Lieberman, D. E. A wider pelvis does not increase locomotor cost in humans, with implications for the evolution of childbirth. *PLoS ONE* **10**, e0118903, doi:10.1371/journal.pone.0118903 (2015).

11 Betti, L. & Manica, A. Human variation in the shape of the birth canal is significant and geographically structured. *Proc. R. Soc. B. Biol. Sci.* **285**, 20181807, doi:10.1098/rspb.2018.1807 (2018).

12 Dunsworth, H. M., Warrener, A. G., Deacon, T., Ellison, P. T. & Pontzer, H. Metabolic hypothesis for human altriciality. *Proc. Natl. Acad. Sci. U.S.A.* **109**, 15212–15216 (2012).

13 Kappelman, J. The evolution of body mass and relative brain size in fossil hominids. *J. Hum. Evol.* **30**, 243–276 (1996).

14 Tague, R. G. & Lovejoy, C. O. The obstetric pelvis of A.L. 288-1 (Lucy). *J. Hum. Evol.* **15**, 237–256 (1986).

15 Berge, C., Orban-Segebarth, R. & Schmid, P. Obstetrical interpretation of the australopithecine pelvic cavity. *J. Hum. Evol.* **13**, 573–587 (1984).

16 Häusler, M. & Schmid, P. Comparison of the pelves of Sts 14 and AL 288-1: implications for birth and sexual dimorphism in australopithecines. *J. Hum. Evol.* **29**, 363–383 (1995).

17 Brassey, C. A., O'Mahoney, T. G., Chamberlain, A. T. & Sellers, W. I. A volumetric technique for fossil body mass estimation applied to Australopithecus afarensis. *J. Hum. Evol.* **115**, 47–64, doi:10.1016/j.jhevol.2017.07.014 (2018).

18 Berge, C. & Goularas, D. A new reconstruction of Sts 14 pelvis (*Australopithecus africanus*) from computed tomography and three-dimensional modeling techniques. *J. Hum. Evol.* **58**, 262–272, doi:10.1016/j.jhevol.2009.11.006 (2010).

19 Kibii, J. M. *et al.* A partial pelvis of *Australopithecus sediba*. *Science* **333**, 1407–1411, doi:10.1126/science.1202521 (2011).

20 Laudicina, N. M., Rodriguez, F. & DeSilva, J. M. Reconstructing birth in *Australopithecus sediba*. *PLoS One* **14**, e0221871, doi:10.1371/journal.pone.0221871 (2019).

21 Gunz, P. *et al. Australopithecus afarensis* endocasts suggest ape-like brain organization and prolonged brain growth. *Sci. Adv.* **6**, eaaz4729, doi:10.1126/sciadv.aaz4729 (2020).

22 Martin, R. D. *Human Brain Evolution in an Ecological Context – 52nd James Arthur Lecture on the Evolution of the Human Brain*. (American Museum of Natural History, 1983).

23 DeSilva, J. M. & Lesnik, J. J. Brain size at birth throughout human evolution: A new method for estimating neonatal brain size in hominins. *J. Hum. Evol.* **55**, 1064–1074 (2008).

24 Stoller, M. K. *The Obstetric Pelvis and Mechanism of Labor in Nonhuman Primates* PhD thesis, University of Chicago, (1995).

25 Lovejoy, C. O., Suwa, G., Spurlock, L., Asfaw, B. & White, T. D. The pelvis and femur of *Ardipithecus ramidus*: the emergence of upright walking. *Science* **326**, 71, doi:10.1126/science.1175831 (2009).

26 Chor, C. M., Chan, W. Y. W., Tse, W. T. A. & Sahota, D. S. Measurement of retropubic tissue thickness using intrapartum transperineal ultrasound to assess cephalopelvic disproportion. *Ultrasonography* **37**, 211–216, doi:10.14366/usg.17003 (2018).

27 Ami, O. *et al.* Three-dimensional magnetic resonance imaging of fetal head molding and brain shape changes during the second stage of labor. *PLoS ONE* **14**, e0215721, doi:10.1371/journal.pone.0215721 (2019).

28 Borell, U. & Fernström, I. Die Umformung des kindlichen Kopfes während normaler Entbindung in regelrechter Hinterhauptslage. *Geburtshilfe Frauenheilkd.* **18**, 1156–1166 (1958).

29 Schultz, A. H. *The Life of Primates*. (Weidenfeld and Nicolson, 1969).

30 Holloway, R. L., Broadfield, D. C. & Carlson, K. J. New high-resolution computed tomography data of the Taung partial cranium and endocast and their bearing on metopism and hominin brain evolution. *Proceedings of the National Academy of Sciences* **111**, 13022–13027, doi:10.1073/pnas.1402905111 (2014).

31 Schultz, A. H. in *Contributions to Embryology, Vol. 28* Vol. 525 1–63 (Carnegie Institute Publication, 1940).

32 Todd, T. W. Age changes in the pubic bone. V. Mammalian public metamorphosis. *Am. J. Phys. Anthropol.* **4**, 333-406, doi:10.1002/ajpa.1330040402 (1921).

33 Becker, I., Woodley, S. J. & Stringer, M. D. The adult human pubic symphysis: a systematic review. *J. Anat.* **217**, 475–487, doi:10.1111/j.1469-7580.2010.01300.x (2010).

34 Reitter, A. *et al.* Does pregnancy and/or shifting positions create more room in a woman's pelvis? *Am. J. Obstet. Gynecol.* **211**, 662.e661, doi:10.1016/j.ajog.2014.06.029 (2014).

35 Michel, S. C. *et al.* MR obstetric pelvimetry: effect of birthing position on pelvic bony dimensions. *AJR. Am. J. Roentgenol.* **179**, 1063–1067, doi:10.2214/ajr.179.4.1791063 (2002).

36 Mink, J. W., Blumenschine, R. J. & Adams, D. B. Ratio of central nervous system to body metabolism in vertebrates: its constancy and functional basis. *Am. J. Physiol.* **241**, R203-212, doi:10.1152/ajpregu.1981.241.3.R203 (1981).

37 Webb, N. M., Fornai, C., Krenn, V. A. & Haeusler, M. Do chimpanzees really have a spacious birth canal? A reanalysis of cephalopelvic proportions and implications for the obstetrical dilemma in humans. *Am. J. Phys. Anthropol. Suppl.* **71**, 111–112 (2021).

38 Haile-Selassie, Y. *et al.* An early *Australopithecus afarensis* postcranium from Woranso-Mille, Ethiopia. *Proc. Natl. Acad. Sci. U.S.A.* **107**, 12121–12126, doi:10.1073/pnas.1004527107 (2010).

39 Haeusler, M. & Ruff, C. B. in *Hominin Postcranial Remains from Sterkfontein, South Africa, 1936–1995 Advances in Human Evolution series* (eds B. Zipfel, B. G. Richmond, & C. V. Ward) 181–201 (Oxford University Press, 2020).

40 Leutenegger, W. Beziehungen zwischen der Neugeborenengrösse und Sexualdimorphismus am Becken bei simischen Primaten. *Folia Primatol.* **12**, 224–235 (1970).

41 Hrdy, S. in *Attachment and bonding: a new synthesis. 92nd Dahlem Workshop Report* (eds C. S. Carter *et al.*) 9–32 (MIT Press, 2005).

42 Isler, K. & van Schaik, C. P. How our ancestors broke through the gray ceiling: comparative evidence for cooperative breeding in early *Homo*. *Curr. Anthrop.* **53**, S453–S465, doi:10.1086/667623 (2012).

43 Kaplan, H., Hill, K., Lancaster, J. & Hurtado, A. M. A theory of human life history evolution: Diet, intelligence, and longevity. *Evolutionary Anthropology: Issues, News, and Reviews* **9**, 156–185, doi:10.1002/1520-6505(2000)9:4<156::Aid-evan5>3.0.Co;2-7 (2000).

44 Hublin, J.-J., Neubauer, S. & Gunz, P. Brain ontogeny and life history in Pleistocene hominins. *Philosophical Transactions of the Royal Society of London B: Biological Sciences* **370**, 20140062, doi:10.1098/rstb.2014.0062 (2015).

45 Harmand, S. *et al.* 3.3-million-year-old stone tools from Lomekwi 3, West Turkana, Kenya. *Nature* **521**, 310–315, doi:10.1038/nature14464 (2015).

46 Leutenegger, W. Neonatal brain size and neurocranial dimensions in Pliocene hominids: implications for obstetrics. *J. Hum. Evol.* **16**, 291 – 296 (1987).

47 Frémondière, P. *L'évolution de l'accouchement dans la lignée humaine. Estimation de la contrainte foeto-pelvienne par deux méthodes complémentaires: la simulation numérique de l'accouchement et l'analyse discriminante des modalités d'accouchement au sein d'un échantillon obstétrical* PhD thesis, Aix-Marseille Université, (2015).

48 Lapeer, R. J. & Prager, R. W. Fetal head moulding: finite element analysis of a fetal skull subjected to uterine pressures during the first stage of labour. *J. Biomech.* **34**, 1125–1133, doi:10.1016/S0021-9290(01)00070-7 (2001).

49 Pu, F. *et al.* Effect of different labor forces on fetal skull molding. *Med. Eng. Phys.* **33**, 620–625, doi:10.1016/j.medengphy.2010.12.018 (2011).

50 Almarza, A. J. & Athanasiou, K. A. Design characteristics for the tissue engineering of cartilaginous tissues. *Ann. Biomed. Eng.* **32**, 2–17, doi:10.1023/b:Abme.0000007786.37957.65 (2004).

51 Ami, O. *et al.* Détection des disproportions fœtopelviennes par réalité virtuelle: étude de faisabilité à propos de trois cas. *J. Radiol.* **92**, 40–45 (2011).

52 Cuppone, M., Seedhom, B. B., Berry, E. & Ostell, A. E. The longitudinal Young's modulus of cortical bone in the midshaft of human femur and its correlation with CT scanning data. *Calcif. Tissue Int.* **74**, 302-309, doi:10.1007/s00223-002-2123-1 (2004).

53 Ohlsén, H. Moulding of the pelvis during labour. *Acta Radiologica Diagnosis* **14**, 417–434 (1973).

54 Borell, U. & Fernström, I. The movements at the sacro-iliac joints and their importance to changes in the pelvic dimensions during paturition. *Acta Obsterica et Gynecologica Scandinaviae* **36**, 42–57 (1957).

55 Hao, Z., Wan, C., Gao, X. & Ji, T. The effect of boundary condition on the biomechanics of a human pelvic joint under an axial compressive load: a three-dimensional finite element model. *J. Biomech. Eng.* **133**, 101006, doi:10.1115/1.4005223 (2011).

56 Mitteroecker, P., Huttegger, S. M., Fischer, B. & Pavlicev, M. Cliff-edge model of obstetric selection in humans. *Proceedings of the National Academy of Science USA* **113**, 14680–14685, doi:10.1073/pnas.1612410113 (2016).

57 Huseynov, A. *et al.* Developmental evidence for obstetric adaptation of the human female pelvis. *Proc. Natl. Acad. Sci. U.S.A.* **103**, 5227–5232, doi:10.1073/pnas.1517085113 (2016).

58 Wells, J. C. K. The new “Obstetrical Dilemma”: stunting, obesity and the risk of obstructed labour. *The Anatomical Record* **300**, 716–731, doi:10.1002/ar.23540 (2017).

59 Krenn, V. A., Fornai, C., Webb, N. M. & Haeusler, M. Sex determination accuracy in a Central European sample using the human sacrum. *Anthropol. Anz.* (in press).

60 Libby, J. *et al.* Modelling human skull growth: a validated computational model. *J R Soc Interface* **14**, doi:10.1098/rsif.2017.0202 (2017).

61 Marchand, F. Über das Hirngewicht des Menschen. *Abhandlungen der Mathematisch-Physischen Classe der Königlich Sächsischen Gesellschaft der Wissenschaften zu Leipzig. Leipzig: Teubner* **27**, 393—482 (1902).

62 Bischoff, T. L. W., von. *Das Hirngewicht des Menschen: eine Studie*. (Neusser, 1880).

63 Bamberg, C. *et al.* Human birth observed in real-time open magnetic resonance imaging. *Am. J. Obstet. Gynecol.* **206**, 505.e501–505.e506, doi:10.1016/j.ajog.2012.01.011 (2012).

64 Bamberg, C. *et al.* Evaluating fetal head dimension changes during labor using open magnetic resonance imaging. *J. Perinat. Med.* **45**, 305–308, doi:10.1515/jpm-2016-0005 (2017).

65 Maran, J. C. *et al.* Comparative anatomy on 3-D MRI of the urogenital sinus and the periurethral area before and during the second stage of labor during childbirth. *Surg. Radiol. Anat.* **40**, 371–380, doi:10.1007/s00276-017-1925-9 (2018).

66 Borell, U. & Fernström, I. Die Umformung des kindlichen Kopfes bei engem Becken. *Geburtshilfe Frauenheilkd.* **18**, 1245–1256 (1958).

67 Carlson, K. J. *et al.* The endocast of MH1, *Australopithecus sediba*. *Science* **333**, 1402–1407, doi:10.1126/science.1203922 (2011).

68 Martin, R. D. *Primate Origins and Evolution*. (Chapman and Hall, 1990).

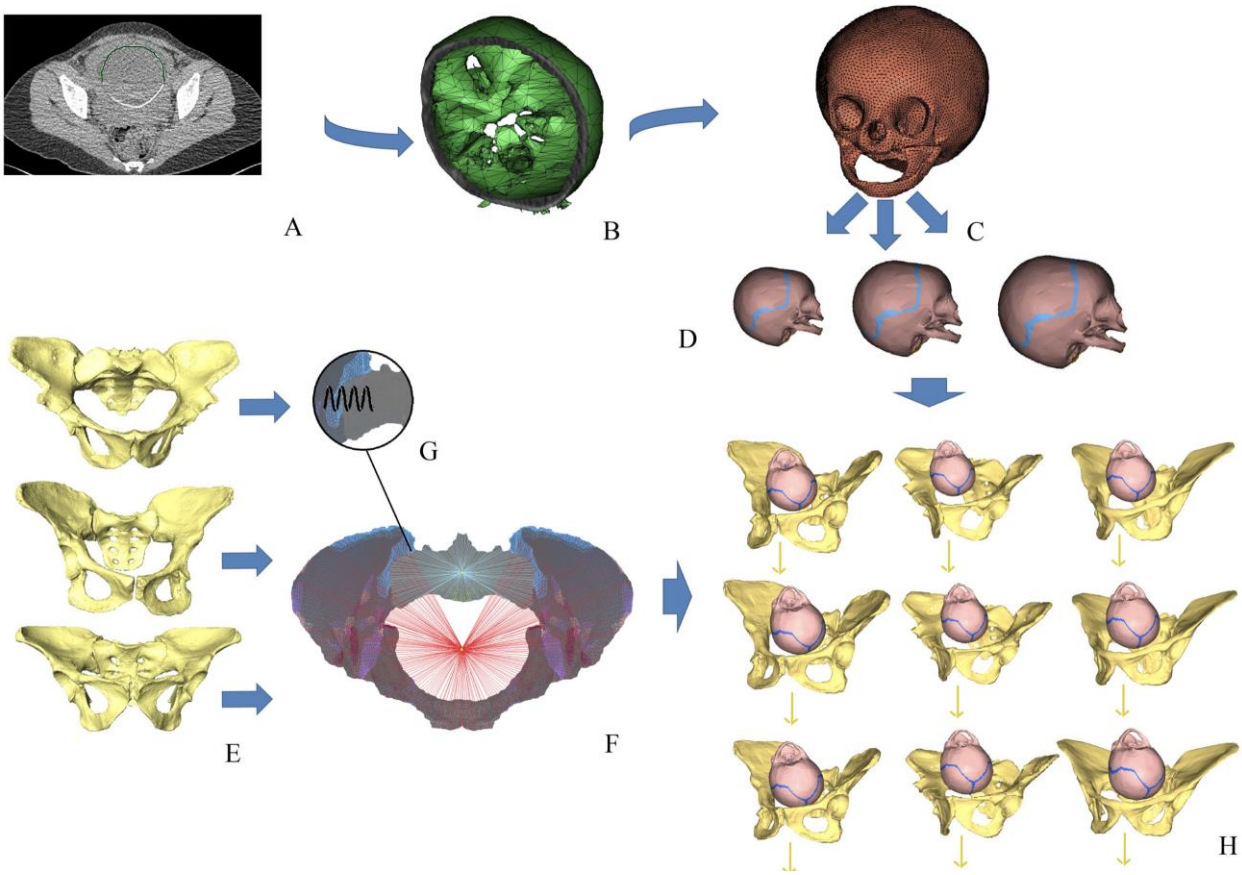

Fig. 1. Workflow for modelling the australopithecine mother-infant dyads. A: segmentation of the fetal skull out of the mother's pelvic CT scan; **B:** generation of a 3D model of the fetal skull; **C:** re-meshing to generate shell elements and to apply the material proprieties of the fontanels and skull; **D:** warping of the fetal skull based on three brain sizes: 110g, 145g and 180g; **E:** pelvis reconstructions of A.L. 288-1, MH2 and Sts 14; **F:** data setting for the pelvic meshes including assignment of material properties and bounding conditions; **G:** representation of the sacro-iliac joint with a spring allowing nutation; **H:** combination of skulls and pelvic meshes leading to a total of 24 mother-fetus dyads, and application of gravity as the force of descent on the skull meshes.

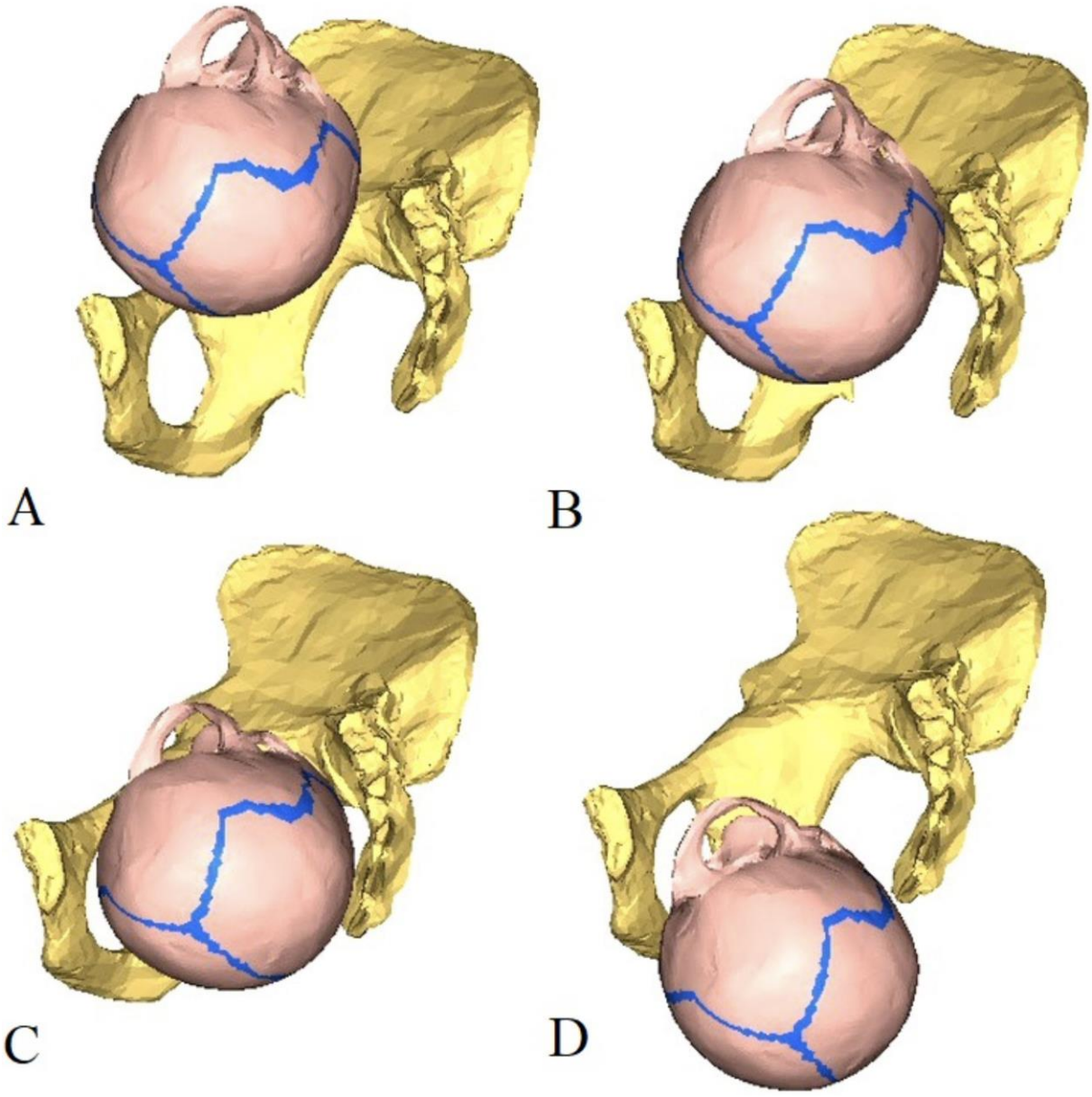

Fig. 2. Phases of bony birth simulation. A fetal head with a 145 g brain size passes through the pelvis of Sts 14 as reconstructed by Häusler and Schmid[16], depicted in lateral view. **A:** Position of the fetal head at the onset of the simulation in right occipito-anterior position; **B:** engagement of the head at the pelvic inlet level; **C:** descent through the pelvic midplane after slight rotation; **D:** expulsion from the outlet with backward nutation of the sacrum by 11 mm. Only the left hipbone and the sacrum are shown for visualization purposes.

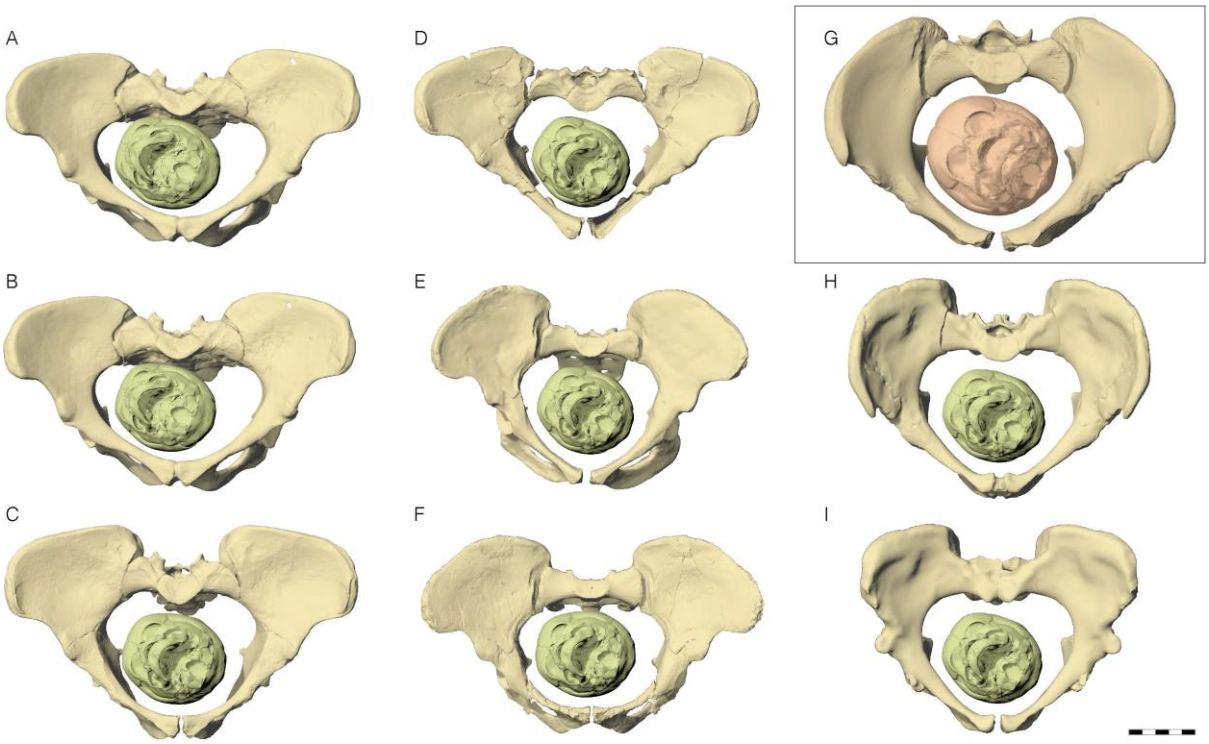

Fig. 3. Australopithecine pelvic reconstructions with a 110 g fetal head size engaged in the pelvic inlet, including A.L. 288-1 (*Australopithecus afarensis*), Sts 14 (*A. africanus*), and MH2 (*A. sediba*), compared to an average sized modern human female pelvis and fetal head (inset, G). A.L. 288-1: A, Lovejoy et al.[25], B, Tague and Lovejoy[14], C, Häusler and Schmid[16], D, Brassey et al.[17]; Sts 14: E, Häusler and Schmid[16], F, Berge and Goularas[18]; MH2: H, Kibii et al.[19], I, Laudicina et al.[20]. All pelves are seen in a view perpendicular to the pelvic inlet. Scale bar 5 cm.

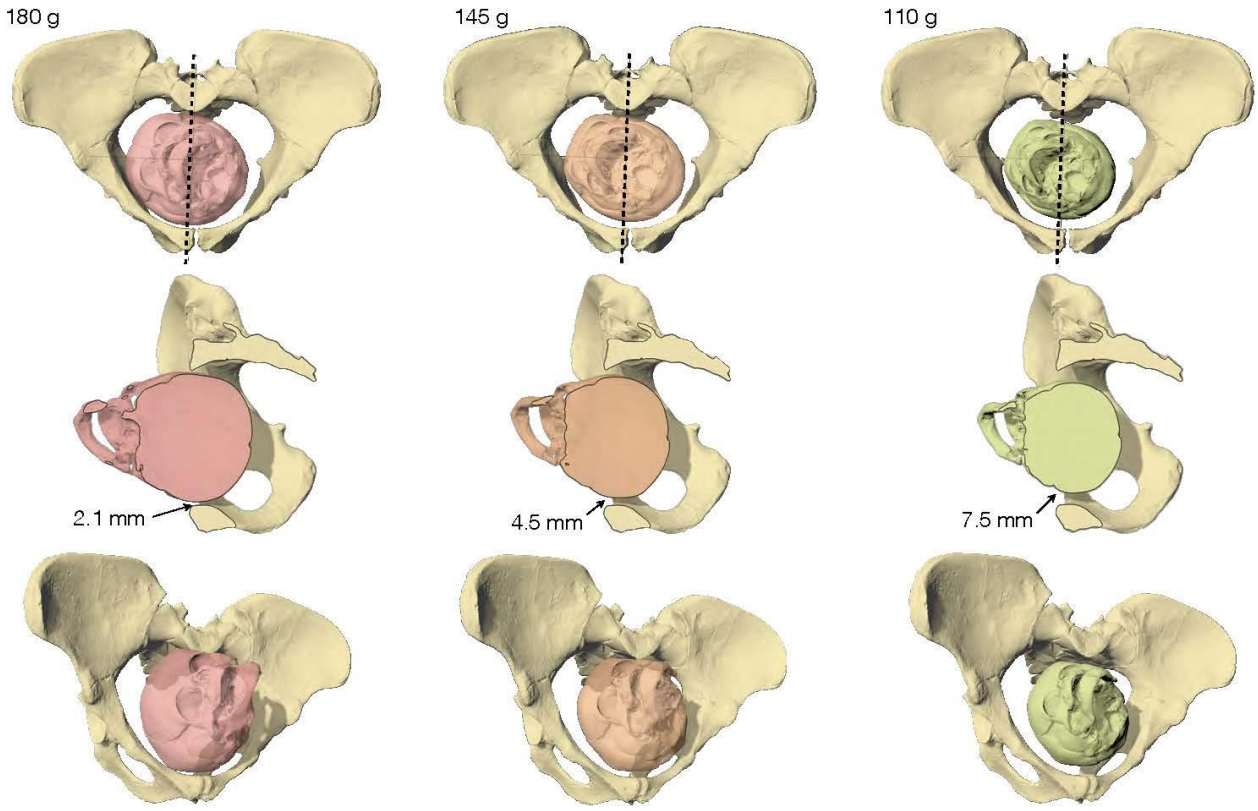

Fig. 4 Engagement of the fetal head in the pelvic inlet in A.L. 288-1, pelvic reconstruction of Häusler & Schmid[16]. The in silico simulation shows that only the 110 g fetal head size leaves sufficient space (i.e., > 7–10.6 mm) for fetopelvic soft tissue. The best cephalopelvic fit is obtained with a slightly oblique head presentation at the pelvic inlet, and the maximum constriction occurs in a para-sagittal plane (dashed line). Top row: view perpendicular to pelvic inlet. Middle row: right lateral view, clipped at the plane of maximum constriction; the figures indicate the width of the gap between the fetal skull and the maternal pelvis. Bottom row: oblique perspective view.

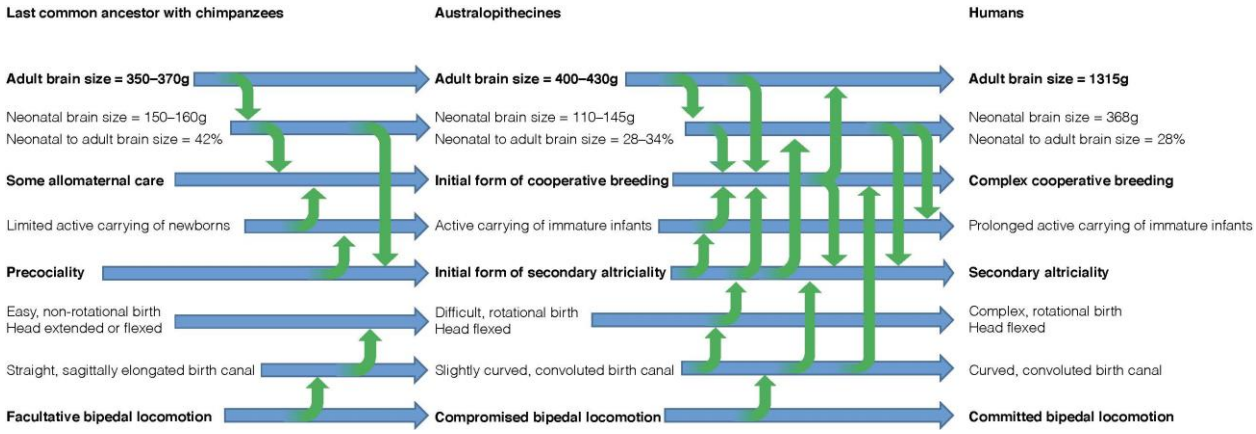

Fig. 5. Obstetrically relevant evolutionary changes during hominin evolution and their interrelationship with locomotion and encephalization. The last common ancestor of humans and great apes probably exhibited a relatively straight birth canal that became antero-posteriorly narrowed and convoluted in australopithecines and modern humans as an adaptation to bipedal locomotion. This led to an increase in the complexity of birth and the evolution of secondary altriciality in *Australopithecus*. The neurologically immature newborn had to be carried by family members, thus necessitating the evolution of cooperative breeding, which was an exaptation for brain size enlargement in *Homo*. Bold font: main characteristics; blue arrows: evolutionary changes; green arrows: influencing factors.

Table 1. Obstetrical analysis of the finite element simulations of the combinations of pelves and neonatal skulls

Pelvic reconstruction	Pelvic inlet area [cm^2]	Pelvic inlet AP [mm]	Pelvic inlet TV [mm]	Neonatal brain size [grams]	Delivery outcome of bony simulations	Level of arrest	Rotation	Nutation [mm] †	Cephalo-pelvic gap at inlet [mm]	Delivery outcome taking soft tissue into account
A.L. 288-1 (Lovejoy et al.) [25]	79	72.4	128	110	eutocic	-	45°	20	3.9	dystocic
				145	dystocic	inlet	90°	-	0.9	dystocic
				180	dystocic	inlet	45°	-	0.0	dystocic
A.L. 288-1 (Tague & Lovejoy) [14]	83	76	132	110	eutocic	-	45°	20	5.5	dystocic
				145	eutocic	-	45°	20	3.0	dystocic
				180	dystocic	inlet	45°	-	0.2	dystocic
A.L. 288-1 (Haeusler & Schmid) [16]	86	81	123	110	eutocic	-	145°	12	7.5	**eutocic**
				145	eutocic	-	45°	12	4.5	dystocic
				180	dystocic	inlet-	45°	-	2.1	dystocic
A.L. 288-1 (Brassey et al.) [17]	79	80	128.5	110	eutocic	-	0°	0	7.0	**eutocic**
				145	eutocic	-	45°	6	4.3	dystocic
				180	dystocic	inlet	0°	-	0.5	dystocic
Sts 14 (Haeusler & Schmid) [16]	72	89	101	110	eutocic	-	45°	11	7.6	**eutocic**
				145	eutocic	-	45°	11	5.9	dystocic
				180	dystocic	midplane	45°	-	3.4	dystocic
Sts 14 (Berge & Goularas) [18]	77	83	116.8	110	eutocic	-	135°	20	8.6	**eutocic**
				145	eutocic	-	90°	20	6.2	dystocic
				180	dystocic	midplane	45°	-	2.7	dystocic
MH2 (Kibii et al. and Laudicina et al.) [19,20]	87	81.7	117.6	110	eutocic	-	90°	8	8.0	**eutocic**
				145	eutocic	-	45°	13	5.1	dystocic
				180	dystocic	inlet	45°	-	2.0	dystocic

† Nutation represents the outlet stretching or backward rotation of the caudal tip of the sacrum

Extended Data

Extended Data Table 1. Adult and neonatal head size estimates based on adult-to-neonatal brain size proportions using different formulas

Species	Adult endocranial volume [cm^3]	Adult brain mass [grams] §	Neonatal brain mass using human relationship [grams] ‖	Neonatal brain mass using general primate formula [grams] #	Neonatal brain mass using catarrhine primate formula [grams] ¶
A. afarensis	445 (N=4) *	419	117	176	164
A. africanus	459 (N=8) †	432	121	184	168
A. sediba	420 (N=1) ‡	396	111	166	157

*based on A.L. 288-1 (dated to 3.18 Ma), A.L. 822-1 (dated to ~3.1 Ma), A.L. 333-45 (dated to ~3.2 Ma), A.L. 444-2 (dated to ~3.0 Ma)[21]

† based on MLD 1 (dated to 2.58–3.0 Ma), MLD 37/38 (dated to 2.58 Ma), Sts 5, Sts 19, Sts 60, Sts 71, StW 505 (all dated to 2.1–2.6 Ma), and Taung (dated to 2.58–3.0 Ma)[67]

‡ based on MH1 (dated to 1.98 Ma)[67]

§ Endocranial volume (C) can be transformed into brain weight (E) using the formula $C = 0.94 \times E^{1.02}$ [68]

|| neonatal brain mass = 0.28 × adult brain mass [22], based on a mean neonatal brain mass of 368 g (N=79) and a mean adult brain mass of 1315 g (N = 864 men and 511 women aged 15 to 59 years) [61,62]

Log (neonatal brain mass) = 1.00 × Log (adult brain mass) – 0.37 (r = 0.992, N = 27) [22]

¶ Log (neonatal brain mass) = 0.7246 × Log (adult brain mass) + 0.3146 (r= 0.98, N = 7) [23]

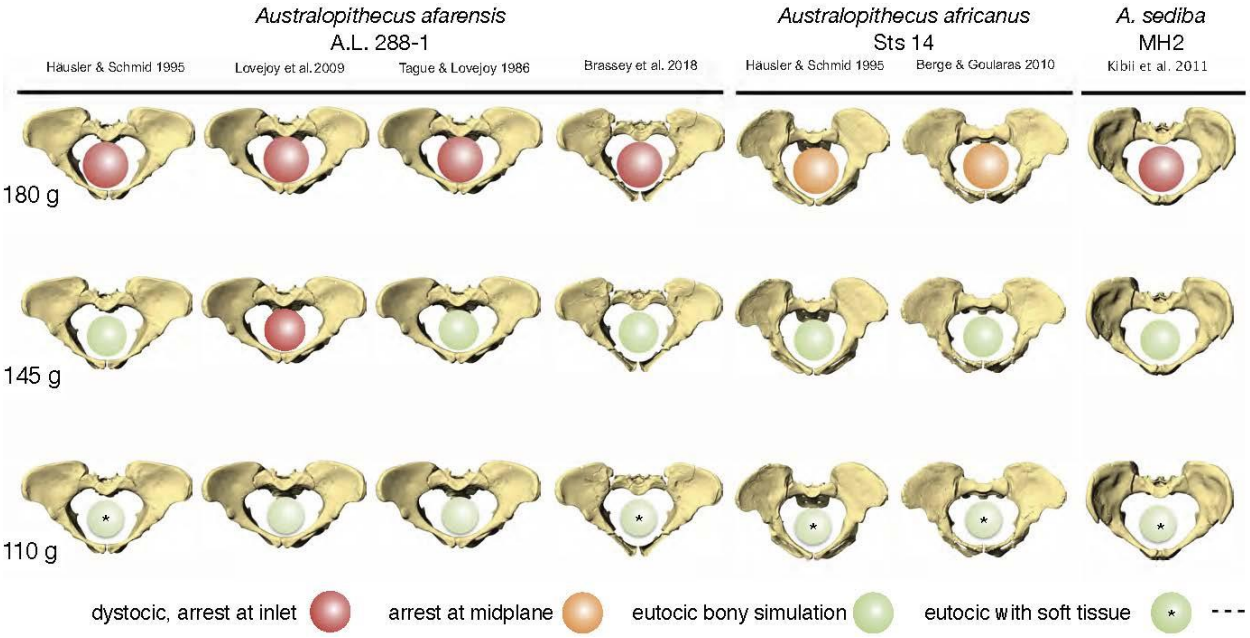

Extended Data Fig. 1. Outcome of bony finite-element (FEA) birth simulations in *Australopithecus*. Simulations based on a 180 g fetal brain size (top), 145 g (middle), 110g (bottom) for the different pelvic reconstructions of A.L. 288-1 (*A. afarensis*)[14,16,17,25], Sts 14 (*A. africanus*)[16,18], and MH2 (*A. sediba*)[19]. The MH2 reconstruction of Laudicina et al.[20] was not included in the FEA simulations because of the incomplete sacrum; otherwise the birth canal dimensions are, however, virtually identical to the reconstruction of Kibii et al.[19]. A red fetal head signifies a dystocic birth with arrest at the pelvic inlet, orange represents an arrest at the midplane, and green color shows an eutocic outcome of the bony simulation, while asterisks mark dyads that are also eutocic if fetopelvic soft tissue thickness is taken into account (i.e., minimum thickness > 7–10.6 mm). View perpendicular to the pelvic inlet, scale bar 5 cm.

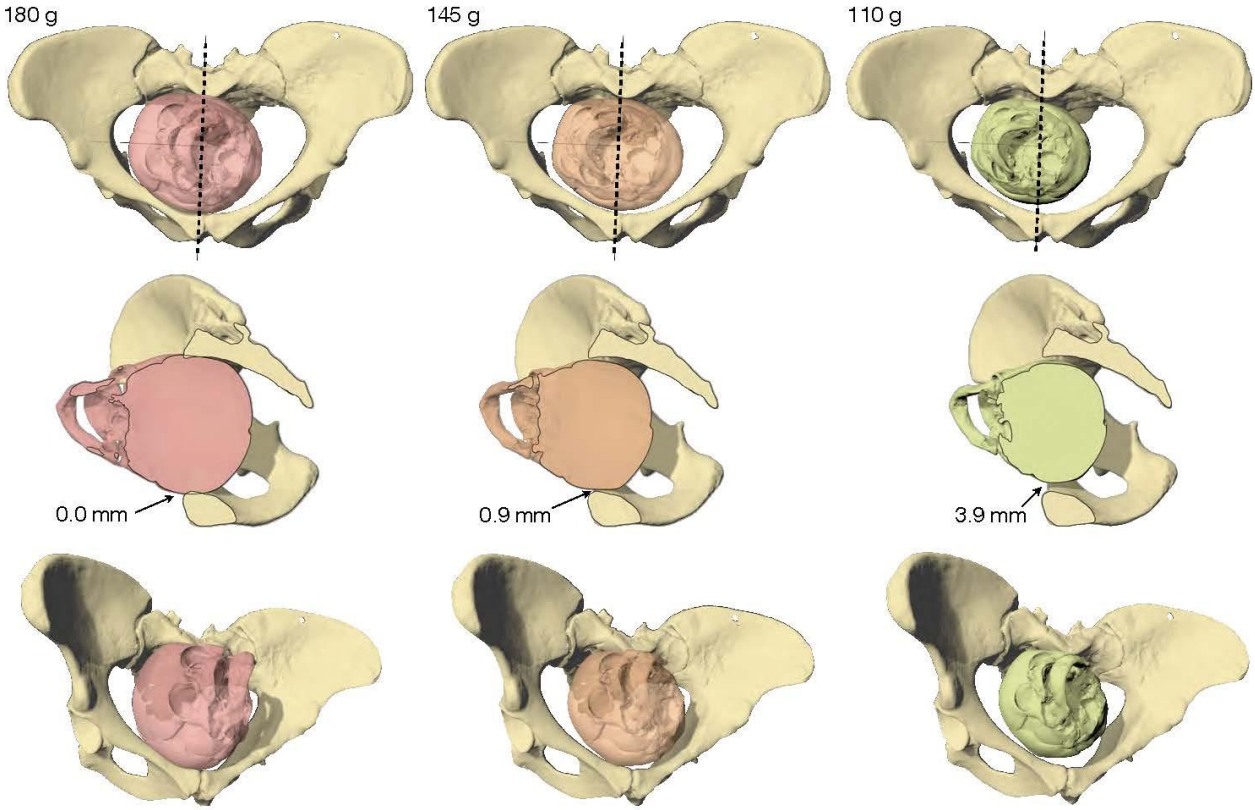

Extended Data Fig. 2 Engagement of the fetal head in the pelvic inlet in A.L. 288-1, pelvic reconstruction of Lovejoy et al.[25]. The in silico simulation shows that none of the three different fetal head sizes leaves sufficient space for fetopelvic soft tissue (i.e., > 7.0–10.6 mm). The best cephalopelvic fit is obtained with a slightly oblique head presentation at the pelvic inlet, and the maximum constriction occurs in a para-sagittal plane (dashed line). Top row: view perpendicular to pelvic inlet. Middle row: right lateral view, clipped at the plane of maximum constriction; the figures indicate the width of the gap between the fetal skull and the maternal pelvis. Bottom row: oblique perspective view.

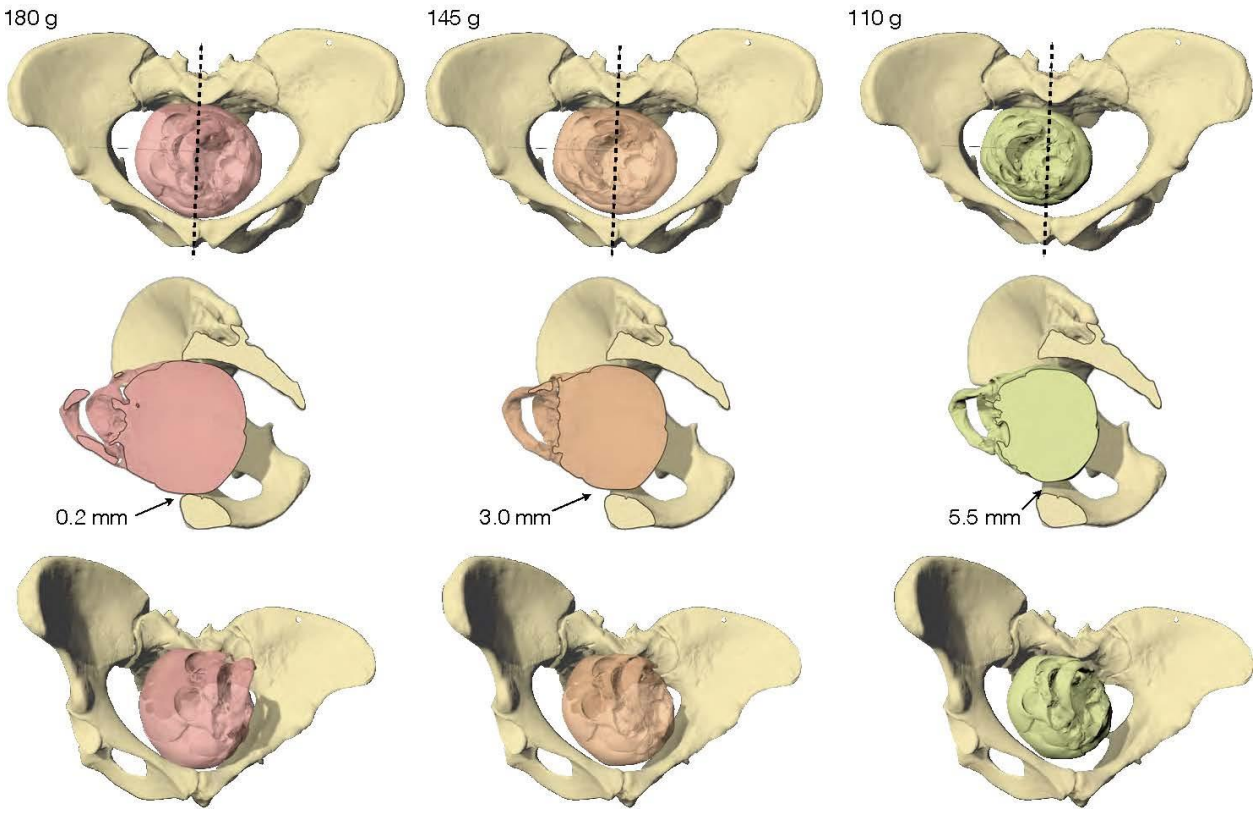

Extended Data Fig. 3. Engagement of the fetal head in the pelvic inlet in A.L. 288-1,Pelvic reconstruction by Tague and Lovejoy[14]. The in silico simulation shows that none of the three different fetal head sizes leaves sufficient space (i.e., > 7.0–10.6 mm) for fetopelvic soft tissue. The best cephalopelvic fit is obtained with a slightly oblique head presentation at the pelvic inlet, and the maximum constriction occurs in a para-sagittal plane (dashed line). Top row: view perpendicular to pelvic inlet. Middle row: right lateral view, clipped at the plane of maximum constriction. Bottom row: oblique perspective view.

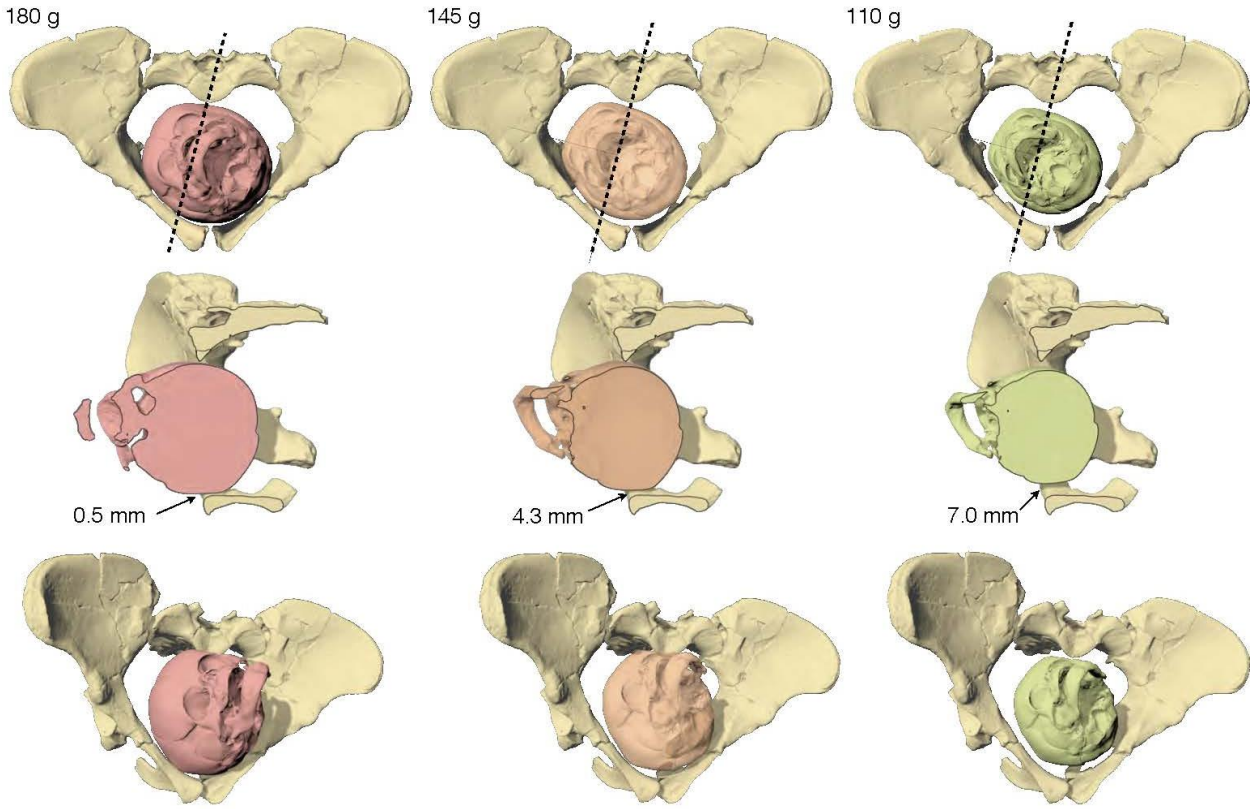

Extended Data Fig. 4 Engagement of the fetal head in the pelvic inlet in A.L. 288-1, pelvic reconstruction of Brassey et al.[17]. The in silico simulation shows that only the 110 g fetal head size leaves sufficient space (i.e., > 7.0–10.6 mm) for fetopelvic soft tissue. The best cephalopelvic fit is obtained with a slightly oblique head presentation at the pelvic inlet, and the maximum constriction occurs in a para-sagittal plane (dashed line). Top row: view perpendicular to pelvic inlet. Middle row: right lateral view, clipped at the plane of maximum constriction; the figures indicate the width of the gap between the fetal skull and the maternal pelvis. Bottom row: oblique perspective view.

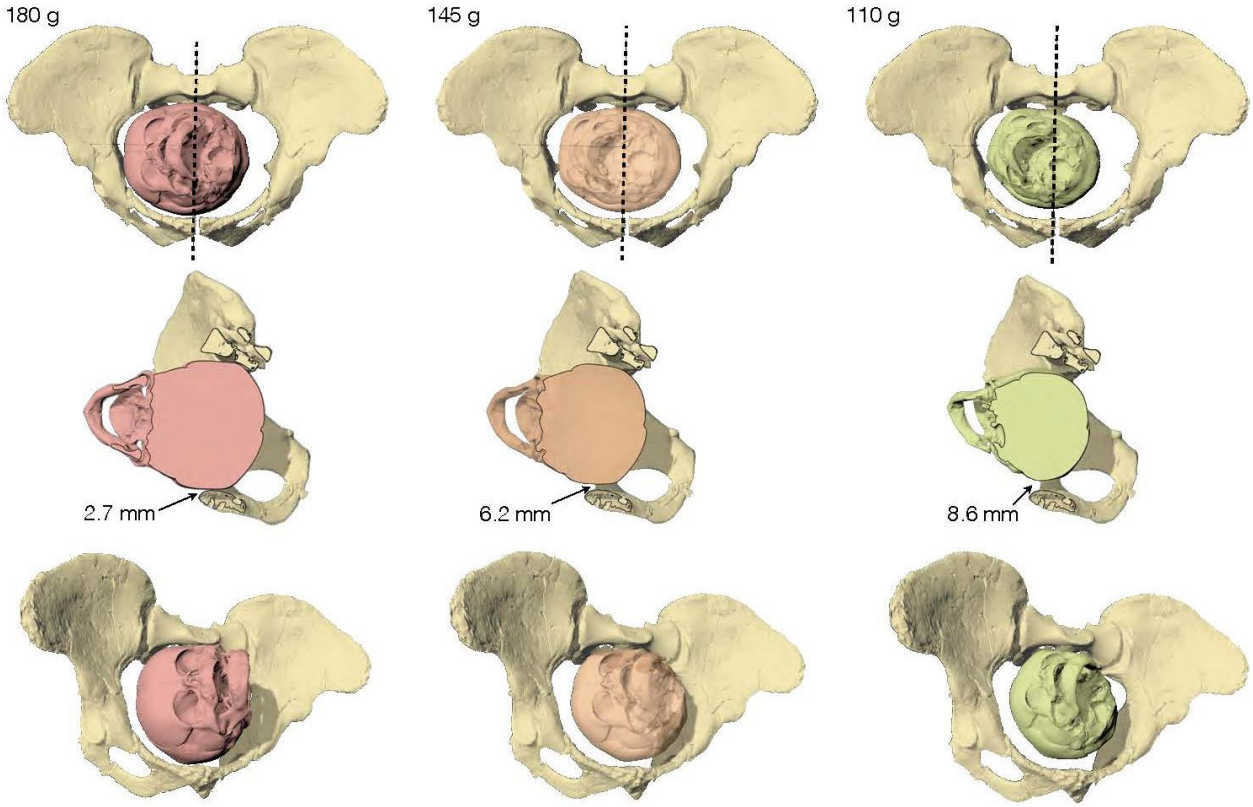

Extended Data Fig. 5 Engagement of the fetal head in the pelvic inlet in Sts 14, pelvic reconstruction of Berge & Goularas[18]. The in silico simulation shows that only the 110 g fetal head size leaves sufficient space (i.e., >7.0–10.6 mm) for fetopelvic soft tissue. The best cephalopelvic fit is obtained with a slightly oblique head presentation at the pelvic inlet, and the maximum constriction occurs in a para-sagittal plane (dashed line). Top row: view perpendicular to pelvic inlet. Middle row: right lateral view, clipped at the plane of maximum constriction; the figures indicate the width of the gap between the fetal skull and the maternal pelvis. Bottom row: oblique perspective view.

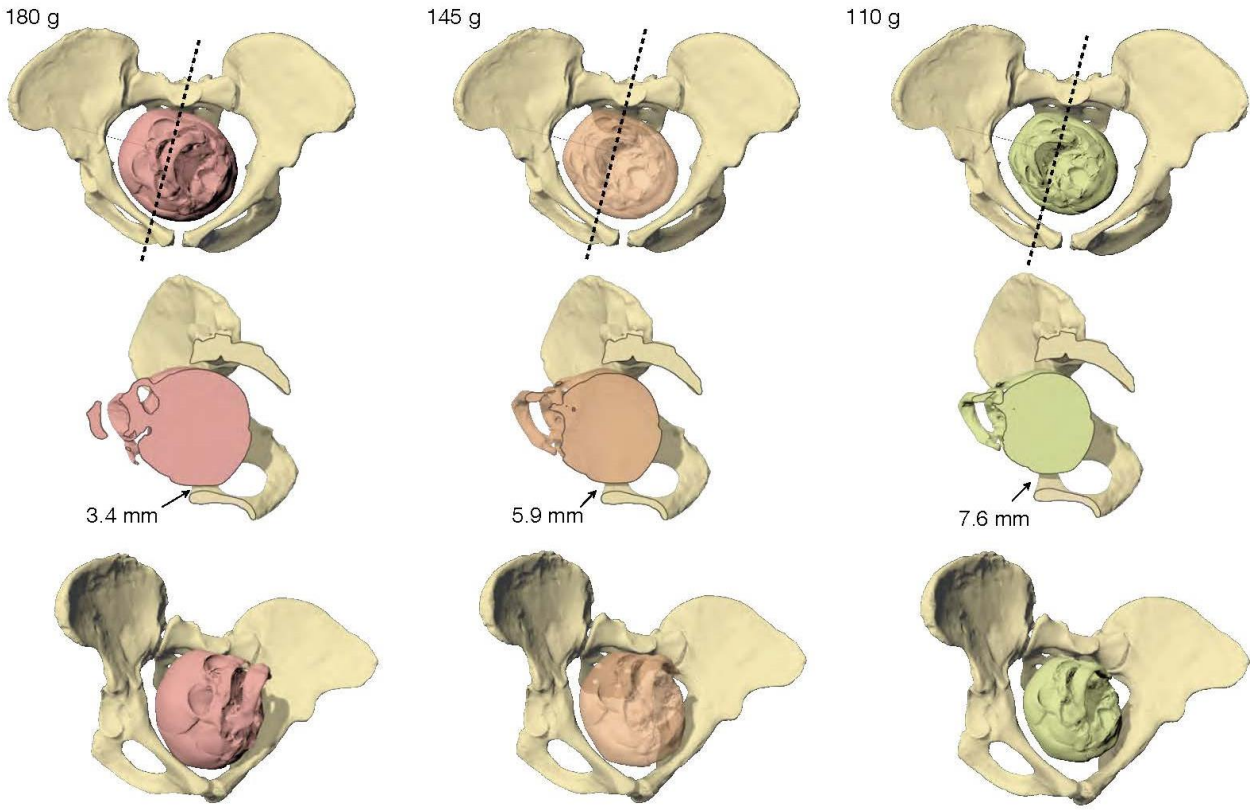

Extended Data Fig. 6 Engagement of the fetal head in the pelvic inlet in Sts 14, pelvic reconstruction of Häusler & Schmid[16]. The in silico simulation shows that only the 110 g fetal head size leaves sufficient space (i.e., > 7.0–10.6 mm) for fetopelvic soft tissue. The best cephalopelvic fit is obtained with a slightly oblique head presentation at the pelvic inlet, and the maximum constriction occurs in a para-sagittal plane (dashed line). Top row: view perpendicular to pelvic inlet. Middle row: right lateral view, clipped at the plane of maximum constriction; the figures indicate the width of the gap between the fetal skull and the maternal pelvis. Bottom row: oblique perspective view.

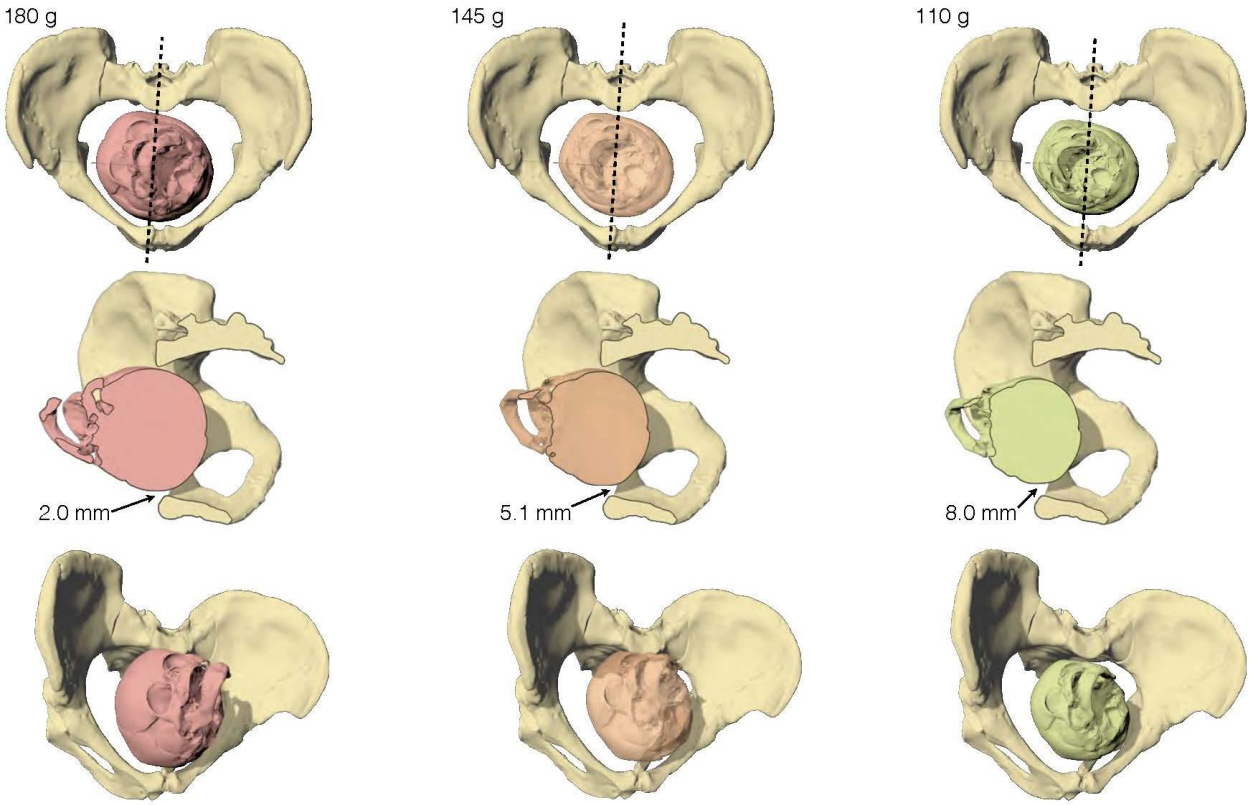

Extended Data Fig. 7 Engagement of the fetal head in the pelvic inlet in MH2, pelvic reconstruction of Kibii et al.[19]. The in silico simulation shows that only the 110 g fetal head size leaves sufficient space (i.e., > 7.0–10.6 mm) for fetopelvic soft tissue. The best cephalopelvic fit is obtained with a slightly oblique head presentation at the pelvic inlet, and the maximum constriction occurs in a para-sagittal plane (dashed line). Top row: view perpendicular to pelvic inlet. Middle row: right lateral view, clipped at the plane of maximum constriction; the figures indicate the width of the gap between the fetal skull and the maternal pelvis. Bottom row: oblique perspective view.

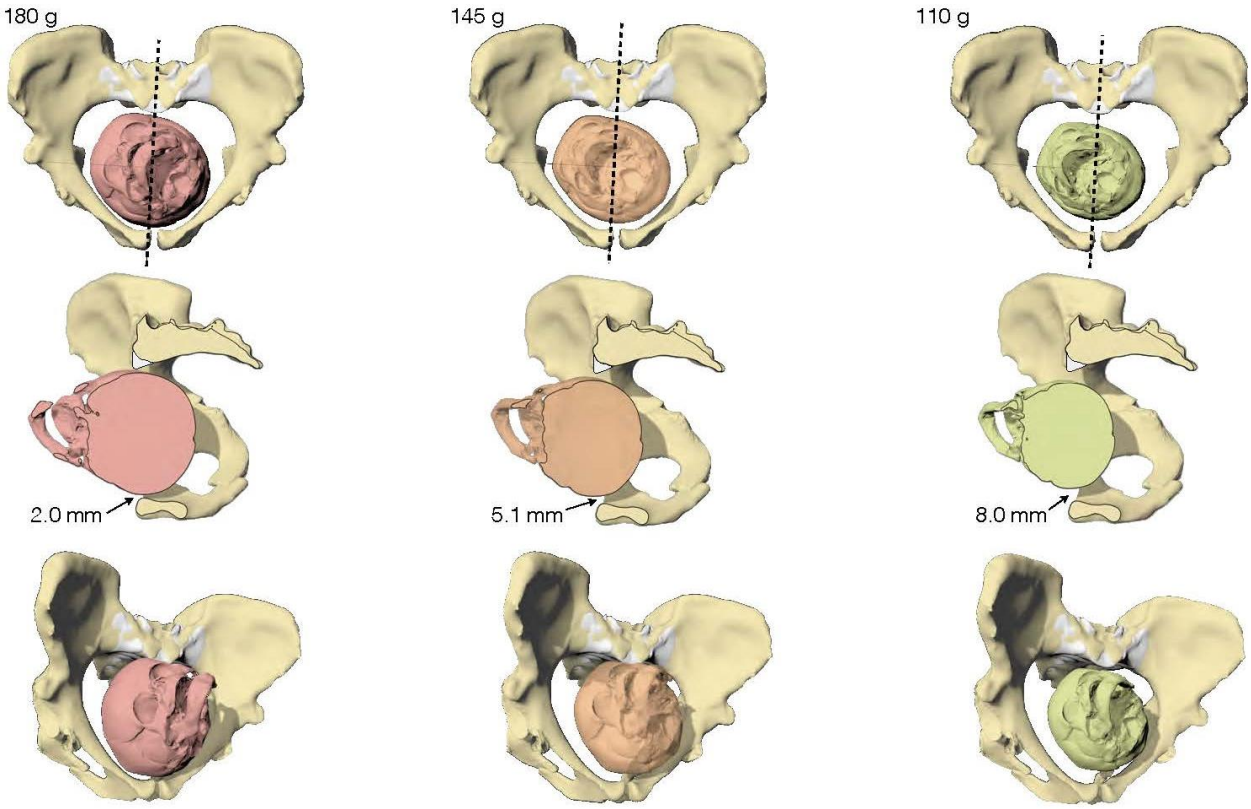

Extended Data Fig. 8 Engagement of the fetal head in the pelvic inlet in MH2, pelvic reconstruction of Laudicina et al.[20]. The sacrum is reconstructed using the sacrum of Kibii et al. [19] (in grey color). The in silico simulation shows that only the 110 g fetal head size leaves sufficient space (i.e., > 7.0–10.6 mm) for fetopelvic soft tissue. The outcome of the in silico simulation is virtually identical to the reconstruction of Kibii et al.[19], and therefore only the latter has been included in the FEA simulations. Top row: frontal view. Middle row: right lateral view, clipped at the plane of maximum constriction; the figures indicate the width of the gap between the fetal skull and the maternal pelvis. Bottom row: oblique perspective view.

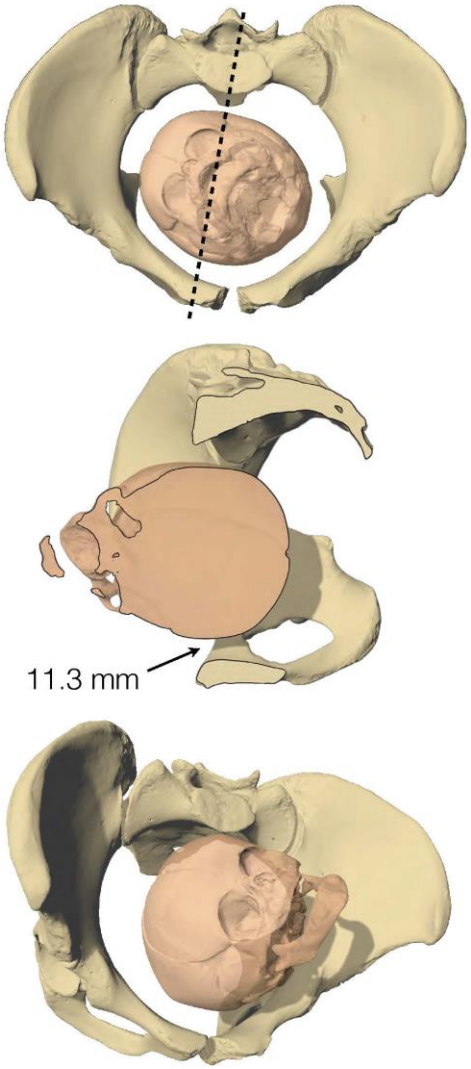

Extended Data Fig. 9 Engagement of the fetal head in the pelvic inlet of a modern human. The pelvis and the fetal skull are scaled to average dimensions (*see Methods*). This suggests that the soft tissue is compressed to a minimum thickness of 11.3 mm between the bony pelvic wall and the fetal skull if the head is centred within the birth canal. Top: view perpendicular to pelvic inlet, a dashed line indicates the plane where maximum constriction occurs. Middle: right lateral view, clipped at the plane of maximum constriction. Bottom: oblique perspective view.

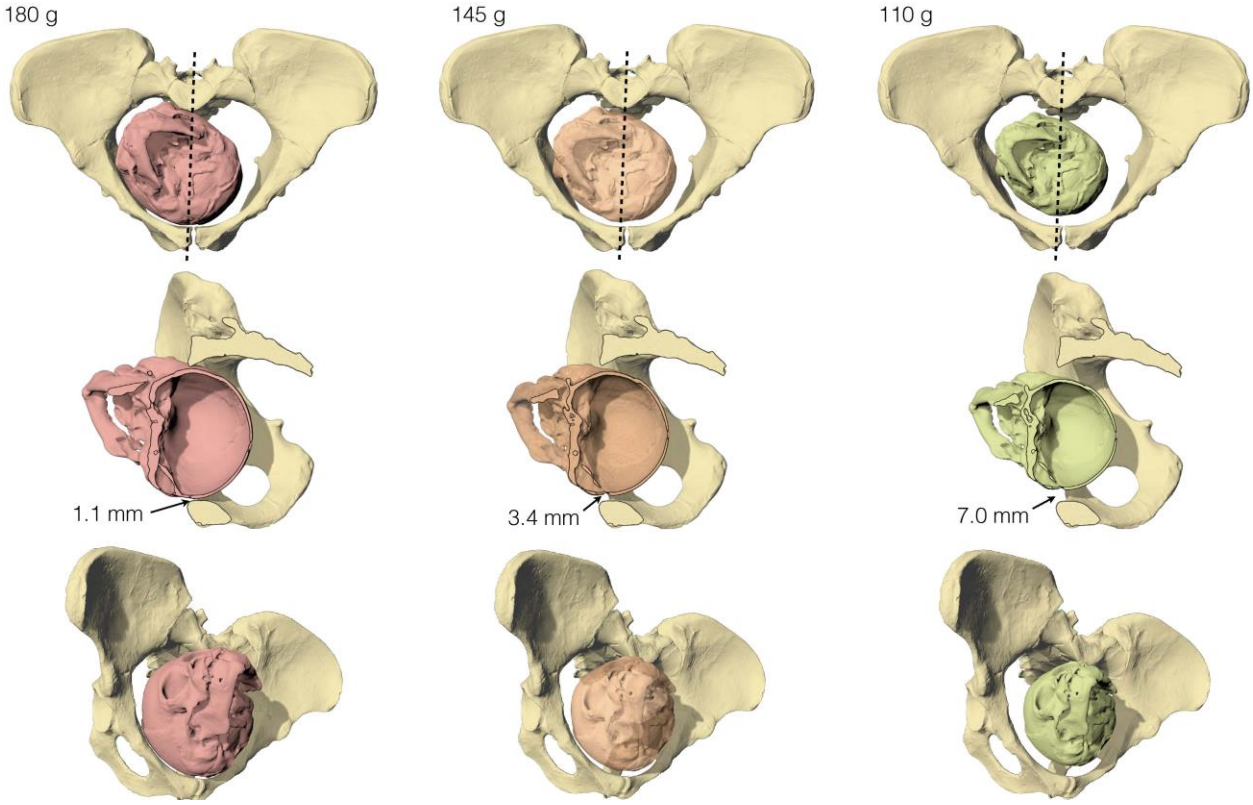

Extended Data Fig. 10 Engagement of a chimpanzee-based fetal head model in the pelvic inlet in A.L. 288-1, pelvic reconstruction of Häusler & Schmid[16]. The in silico simulation shows that only the 110 g fetal head size leaves sufficient space (i.e., > 7.0–10.6 mm) for fetopelvic soft tissue. The best cephalopelvic fit is obtained with a slightly oblique head presentation at the pelvic inlet, and the maximum constriction occurs in a para-sagittal plane (dashed line). Top row: view perpendicular to pelvic inlet. Middle row: right lateral view, clipped at the plane of maximum constriction; the figures indicate the width of the gap between the fetal skull and the maternal pelvis. Bottom row: oblique perspective view.

.

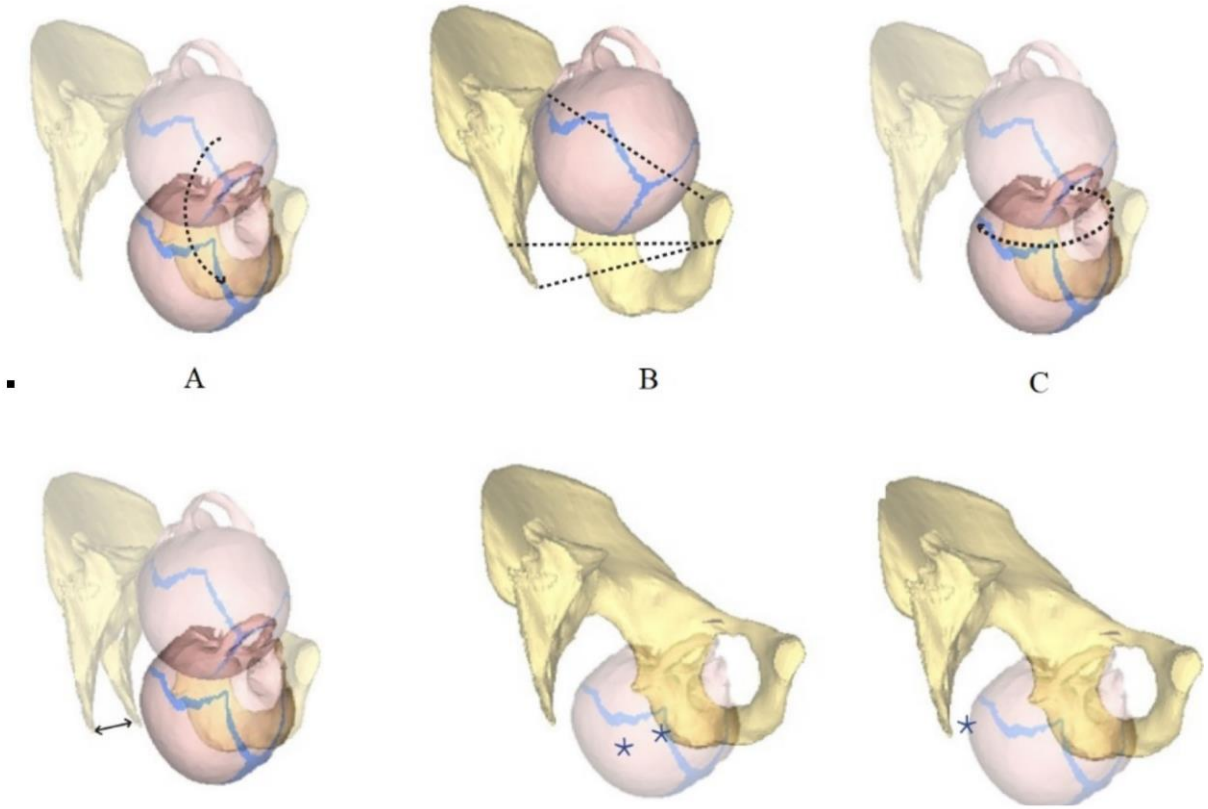

Extended Data Fig. 11. Obstetrical parameters. Lateral views of the maternal pelvic-fetal head dyads during simulation. The right hipbone has been removed for visualization purposes. A: eutocic birth (skull passing through the pelvis) or dystocic (arrest of descent of the skull); B: if birth is dystocic, the level of arrest (pelvic inlet, midplane or outlet; dashed lines); C: rotation of the skull (in degrees); D: the opening of the outlet (outlet stretching) though backward rotation of the sacrum (double arrow); E: position of parietal eminences (left star) with respect to the ischial tuberosities (right star); F: position of the occiput (star) at the outlet.

Supplementary Files

This is a list of supplementary files associated with this preprint. Click to download.

- npreportingsumm002.pdf